Article:

Hofmann, B., Magee, C. orcid.org/0000-0001-9836-2365 and Wright, T.J. (2024) Throw distribution across the Dabbahu-Manda Hararo dike-induced fault array. Geology. ISSN 0091-7613

https://doi.org/10.1130/G52665.1

Throw distribution across the Dabbahu-Manda Hararo dike-induced fault array

Barbara Hofmann[1], Craig Magee[2], Tim J Wright[2]

[1]HR Wallingford, Howbery Park, Wallingford, UK

[2]COMET, School of Earth and Environment, University of Leeds, UK

ABSTRACT

Dike intrusion and formation of overlying dike-induced normal faults facilitate plate extension. The kinematics of these dike-induced normal faults can provide an accessible record of subsurface diking. Here, we use high-resolution LiDAR and InSAR data to explore how strain was distributed across a pre-existing dike-induced fault array during discrete diking events in the Dabbahu-Manda Hararo magmatic segment (Afar, Ethiopia) in 2008 and 2010. By analysing throw of the dike-induced normal faults we show that only a small number of faults were reactivated during each diking event; the distribution of this reactivation likely depended on dike depth, opening, and inclination, as well as fault orientation. We also show fault throw favourably accrued towards fault centers, away from areas of soft- or hard-linkage. Our high-resolution datasets demonstrate the importance of reactivation to rifting, as it means extension can occur at lower extensional forces, and that fault slip (and seismic hazard) may not localise at sites of fault linkage.

INTRODUCTION

When magma is readily available during continental rifting or seafloor spreading, extension is often accommodated by dike emplacement (e.g. Calais et al., 2008; Chadwick and Embley, 1998; Ebinger and Casey, 2001; Pollard et al., 1983; Rubin and Pollard, 1988; Wright et al., 2006). Most dikes do not reach the surface and instead, above a single dike, extension of the overlying rock tends to be accommodated by pairs of normal faults that strike parallel to and dip towards the underlying dike upper tip (e.g. Magee and Jackson, 2020; Mastin and Pollard, 1988; Trippanera et al., 2015a; Trippanera et al., 2015b). Where dikes are closely spaced, complex arrays of these dike-induced normal faults may develop (e.g. Dumont et al., 2017; Dumont et al., 2016; Hjartardóttir et al., 2012; Rowland et al., 2007). Such dike-induced faults also form on and near volcanic edifices (e.g., Bonali et al., 2024; Mastin and Pollard, 1988). Critically, the surface expression of dike-induced faults provides a record of otherwise inaccessible subsurface magmatic and rifting processes, and helps us: (1) unravel how continents break apart and oceanic crust forms (e.g., Chadwick and Embley, 1998; Rowland et al., 2007; Ruch et al., 2016; Wright et al., 2006); (2) track intruding dikes, which aids eruption forecasting (e.g., Pallister et al., 2010); and (3) assess whether or not fault slip, and thus seismic hazard, preferentially localises where faults link (e.g. Walker et al., 2009). However, previous studies typically focus on dike-induced fault pairs above single dikes, with few exploring how the surface expression of complex dike-induced fault arrays evolves (e.g., Dumont et al., 2017; Dumont et al., 2016). Here, we use repeat high-resolution, airborne light detection and ranging (LiDAR) surveys and synthetic aperture radar interferometry (InSAR) data to establish how strain was distributed across a dike-induced normal fault array during two diking events (2008 and 2010) within the Dabbahu-Manda Hararo magmatic segment in Afar, Ethiopia.

GEOLOGICAL SETTING

Extension in magmatic segments in Afar is facilitated by frequent dike intrusions, which are expressed at the surface as arrays of dike-induced normal faults, fissure eruptions, and volcanic centres (e.g. Fig. 1) (e.g. Casey et al., 2006; Ebinger and Casey, 2001; Rowland et al., 2007); this structure is similar to magmatic segments along mid-ocean ridges (e.g. Chadwick and Embley, 1998). Between 2005 and 2010, a series of 14 diking events reactivated portions of a dike-induced normal fault array within the Dabbahu-Manda Hararo magmatic segment (Figs 1 and 2A-B) (e.g. Dumont et al., 2016; Grandin et al., 2010; Hamling et al., 2009; Wright et al., 2012). Modelling of geophysical and geodetic data suggests the 2005 dike intrusion was ~65 km long, opened by up to 8 m at depths of ~2–9 km, and instigated up to ~7 m slip on ≲15 sub-parallel normal faults (Fig. 1) (e.g. Grandin et al., 2009; Grandin et al., 2010; Hamling et al., 2009; Wright et al., 2006). Ground deformation related to the 13 later dike events (2006–2010) can be explained by further diking and fault slip (e.g. Grandin et al., 2010; Hamling, 2010; Hamling et al., 2009). We focus on two dike intrusion events in: (1) October 2008, which likely involved intrusion of a ~11 km long dike with an opening of up to ~3 m (Fig. 2C) (Hamling, 2010); and (2) May 2010 when a ~15 km long dike intrusion, with an opening of up to ~1 m, fed a small lava flow (Fig. 2D) (Barnie et al., 2016).

DATA AND METHODS

We use InSAR and LiDAR data that image the Dabbahu-Manda Hararo magmatic segment. With the InSAR data, we focus on the October 2008 dike event and use track 499 Advanced Land Observing Satellite (ALOS) acquisitions, obtained on 14 September and 15 December 2008, to extract line of site (LOS) displacement trends of the surface at 20 m resolution (Fig. 2C) (Hofmann, 2013). The two LiDAR surveys we use were acquired in October 2009 and November 2012 (Barnie et al., 2016; Hofmann, 2013). Using the original LiDAR point cloud data, we applied an Iterative Closest Point (ICP) algorithm to isolate the vertical and horizontal (in E-W and N-S directions) differences between the 2009 and 2012 surveys (Fig.

3A); combining these allow us to calculate the 3D displacement field related to the May 2010 dike event (Fig. 3B) (e.g. Nissen et al., 2012). We develop an algorithm that for both datasets identify fault hanging wall and footwall cut-offs from changes in LOS displacement or elevation gradients on across-fault profiles (Figs 2B and C; Supplementary Text). Throw is calculated from the identified faults cut-offs but heave, and thus displacement, cannot always be accurately defined where fault monoclines and debris are present (Fig. 2E). To account for various sources of noise in our datasets, we conservatively consider throw values <20 cm may be erroneous. Our analysis is limited as profiles may not always be orthogonal to local fault strike, there is uncertainty regarding fault dip at depth (Magee and Jackson, 2021), and some faults are missed (e.g. Fig. 2C).

RESULTS

We map discrete fault traces, although most are physically connected to (hard-linked) and/or <2 m from (soft-linked) other faults at some point(s), and show their density varies across the area (Fig. 2A). Throw measured across the faults using the 2009 LiDAR data is up to ~140 m (mean of all faults ~14 m), and often appears to increase away from lateral fault tips (Fig. 2B). InSAR data reveal only a selection of these faults were reactivated during the October 2008 diking event, broadly divisible into two fault systems bordering a narrow (~2 km), ~8.5 km long zone of subsidence (Fig. 2C). The western fault system is broader and comprises more, shorter faults than that to the east, where throw is focused onto a few, longer faults (Fig. 2C). Throw accrued along these fault systems, up to ~1.23 m on individual faults, appears to primarily occur towards fault centers (Fig. 2C). Faults between the two active fault systems, within the graben, show little displacement (Fig. 2C).

Our ICP analysis indicates that between acquisition of the October 2009 and November 2012 LiDAR surveys, a ~2 km wide zone of primarily west-dipping, dike-induced normal faults were reactivated, accommodating subsidence of up to ~2 m (Figs 2D-4). Slip vectors reconstructed by combining the ICP derived vertical and horizontal LiDAR difference maps suggest the reactivated faults have a mean plunge of 62±17°, are predominantly dip-slip, and that slip increases away from lateral fault tips (Fig. 3). Some of these vectors, particularly those plunging <30°, may be erroneous due to increased noise within the ICP horizontal displacement data (Hofmann, 2013). Regardless, most reactivated faults are located between the two fault systems that were active during the October 2008 dike event, where little displacement occurred (Figs 2C and D). We recognise 18 key faults that were reactivated, and these can be sub-divided into three fault systems (Fig. 4). Within fault systems 1 and 2, which itself branches into two sub-systems, accrued throw is typically greatest near the centres of individual faults and decreases towards their lateral tips; there are no trends in cumulative throw across each system or no prominent throw increases where faults overlap or link (Fig. 4). Along Fault system 3, cumulative throw defines an approximately elliptical pattern with throw greatest in the system center and decreasing towards its lateral tips (Fig. 4). Across all faults and fault systems clear zones of increased or decreased throw occur (Fig. 4C).

DISCUSSION

In the Dabbahu-Manda Hararo magmatic segment, episodic intrusion of closely spaced dikes has formed a complex array of dike-induced faults and fractures (Fig. 2). InSAR data reveal two localised fault systems were reactivated during the October 2008 diking event, yet faults within the intervening zone of subsidence were not (Fig. 2C) (see also Dumont et al., 2016). This distribution of strain likely occurred because the reactivated faults were favourably oriented and located where dike-induced tensile stresses concentrated (e.g. Pollard et al., 1983; Rubin, 1992; Rubin and Pollard, 1988). Reactivation of shorter faults in the western system compared to the east could be due to: (1) the style of pre-existing faults, with fault density seemingly decreasing towards the Ado'Ale Volcanic Complex (Fig. 2C); and/or (2) the underlying dike dipping westwards (e.g. Barisin et al., 2009), as areas of concentrated tensile stress are larger in the hanging wall of inclined sheets (e.g. Bazargan and Gudmundsson, 2019; Drymoni et al., 2023). In contrast to the October 2008 dike intrusion, the faults reactivated by the May 2010 dike cannot be separated into two parallel systems, and instead occur in one narrow, elongated zone comprising several half-graben (Figs 2D, 3, and 4). This difference in strain distribution between the 2008 and 2010 diking events is likely because the latter dike reached a shallower depth, thus reducing the distance between the tensile stress concentrations at the surface (e.g. Trippanera et al., 2015b). Indeed the May 2010 dike fed a small fissure eruption (Fig. 2D) (Barnie et al., 2016).

Implications

Diking and plate extension

We demonstrate that within complex dike-induced fault arrays, the reactivation of multiple, pre-existing faults seems preferential to formation of new dike-induced faults (Ruch et al., 2016). Critically, less stress is required to reactivate a favourably oriented fault, compared to generating a new fault (e.g. Byerlee, 1978). Our findings thus support analytical and numerical models that suggest diking and associated faulting reduce the extensional forces needed to extend the lithosphere (e.g. Li et al., 2023).

Tracking dikes from surface deformation

Inverting ground deformation data (e.g. from InSAR) allows us to estimate dike and fault locations, geometries, depths, and other properties (e.g., Pallister et al., 2010). In our study area, previously modelled dike and fault locations for the October 2008 and May 2010 events capture the broad surface displacement patterns recorded (Figs 2C and D) (e.g. Grandin et al., 2010; Hamling, 2010; Hamling et al., 2009; Rowland et al., 2007). However, from our observations of surface faulting for the 2008 dike event, we would expect the dike trace to bisect the graben defined by the two active fault systems (Fig. 2C) (cf. Hamling, 2010), consistent with models locating the 2006–2009 dikes slightly west of the 2005 dike (Grandin et al., 2010). For the 2010 event, our data suggests the dike trace should bisect the area of fault activity and occur below the recognised fissure eruption (Fig. 2D) (Barnie et al., 2016). Our work suggests that mapping and quantifying fault and fracture patterns in the field, or from airborne or satellite data, complement and enable ground-truthing of ground deformation models (e.g. Ruch et al., 2016).

Slip distribution along faults

Elastic theories of fault growth suggest throw, a proxy for slip, should be greatest towards fault centres and gradually decay to zero at fault tips (e.g. Rotevatn et al., 2019). Where soft- or hard-linkage between faults occurs, throw is initially low (e.g. Walker et al., 2009; Walsh et al., 2003). Continued slip on linked faults may maintain these local throw minima, or preferentially accrue in these areas, potentially increasing seismic hazard, until the throw gradient across the entire fault homogenises (e.g. Walker et al., 2009). Our data suggests that that during discrete faulting events, throw typically accrues towards fault centers, away from sites of linkage exposed at the surface (Figs 2C, D, and 4); i.e. throw minima at (breached) relays are maintained, supporting similar inferences from normal faults elsewhere (e.g. Walker et al., 2009). It may thus be erroneous to suspect seismic hazard may be increased at sites of fault linkage (e.g. Walker et al., 2009).

CONCLUSIONS

Magmatic diking is common in extensional settings, such as continental rifts and seafloor spreading centres, and at active volcanoes. Because many dikes arrest at depth, their extension often instigates development of overlying normal faults. Where such diking is intense, complex arrays of overlying dike-induced normal faults form. We examine fault throw distribution across such a dike-induced fault array, located in the Dabbahu-Manda Hararo magmatic segment, Afar (Ethiopia), using a combination of LiDAR and InSAR data. We show that intrusion of a dike in October 2008 reactivated two, dike-parallel fault systems bordering an area of subsidence and little deformation. Diking in 2010 reactivated west-dipping faults within the graben that subsided in 2008, but not any of the faults active in 2008. Our results suggest reactivation of dike-induced faults can be an important process in magma-assisted rifting as extension can occur at lower extensional forces. We also show that fault throw typically accrued, during both dike intrusion events, towards faults centers and apparently away from zones of soft- or hard-linkage. Such fault throw distributions questions suggestions that fault slip and seismic hazard are expected to localise where faults link.

ACKNOWLEDGEMENTS

BH was funded by the Leverhulme Trust, NERC Afar Rift Consortium (NE/E007414/1), and BGS through their BUFI programme. CM was funded through a NERC Independent Research Fellowship (NE\R014086\1), and TW through COMET (Centre for the Observation and Modelling of Earthquakes, Volcanoes and Tectonics) and the Royal Society. We thank the NERC Airborne Research and Survey Facility for data collection and provision, and the Institute for Geophysics, Space Science and Astronomy of Addis Ababa University, the Afar Regional government, and the Ethiopian Ministries of Capacity Building, and of Mines and Energy for support.

AUTHOR STATEMENT

BH processed, analysed, and interpreted the data and contributed to article editing. CM contributed to interpretation and led writing. TW planned and acquired the data and aided interpretation and article editing.

DATA AVAILABILITY

The LiDAR data are publicly available (https://data.ceda.ac.uk/neodc/arsf/2008/ET07_04 and https://data.ceda.ac.uk/neodc/arsf/2012/ET12_18), and the InSAR data via https://earth.esa.int/eogateway/catalog/alos-palsar-products. All mapped fault traces and acquired fault displacement data are available from the UK's National Geoscience Data Centre (NGDC), Item ID 182212, at https://www.bgs.ac.uk/geological-data/national-geoscience-data-centre/.

FIGURE CAPTIONS

Figure 1: Location of the Dabbahu-Manda Hararo magmatic segment showing the October (Oct.) 2009 and November (Nov.) 2012 LiDAR surveys, local volcanoes, and normal faults (Vye-Brown et al., 2012). Modelled dike and dike-induced faults are from Wright et al. (2006) and Hamling et al. (2009) for events between 2005 and 2010.

Figure 2: Maps showing: (A) the October 2009 LiDAR data and dike-induced faults (modified from Vye-Brown et al. 2012), with modelled dike and fault traces (e.g. Hamling et al., 2009; Wright et al., 2006); (B) total fault throw calculated from the 2009 LiDAR data; (C) fault throw accrued between September 2008 and December 2008, superimposed on east-west Line-of-Sight (LOS) displacement gradient from an ALOS interferogram; and (D) fault throw measured from a ICP vertical difference (diff.) map of the October 2009 and

November 2012 LiDAR datasets. (E) Schematic showing how we identify footwall and hanging wall cut-off. See Supplementary Figure S1 for uninterpreted version.

Figure 3: (A) Horizontal (E-W and N-S) and vertical differences between the 2009 and 2012 LiDAR surveys, derived using an ICP algorithm. (B) 3D displacements of the dike-induced faults reactivated during the May 2010 dike event (modelled dike trace from Hamling et al., 2009; Wright et al., 2006), shown as slip vectors. We calculate these vectors by modifying our algorithm to extract the vertical and horizontal differences at coincident cut-offs.

Figure 4: (A) Fault throw accrued during the May 2010 diking event (modelled dike trace from Hamling et al., 2009; Wright et al., 2006), which primarily occurred on 18 faults divided into three fault systems. (B) Throw-distance plots for the 18 faults active between the 2009 and 2012 survey acquisitions, when the May 2010 dike intrusion event occurred. (C) Cumulative throw-distance plot showing the cumulative throw accrued along-strike on each fault system, and that acquired by all faults.

References

Barisin, I., Leprince, S., Parsons, B., and Wright, T., 2009, Surface displacements in the September 2005 Afar rifting event from satellite image matching: Asymmetric uplift and faulting: Geophysical Research Letters, v. 36, no. 7.

Barnie, T., Keir, D., Hamling, I., Hofmann, B., Belachew, M., Carn, S., Eastwell, D., Hammond, J. O., Ayele, A., and Oppenheimer, C., 2016, A multidisciplinary study of the final episode of the Manda Hararo dyke sequence, Ethiopia, and implications for trends in volcanism during the rifting cycle: Geological Society, London, Special Publications, v. 420, no. 1, p. 149-163.

Bazargan, M., and Gudmundsson, A., 2019, Dike-induced stresses and displacements in layered volcanic zones: Journal of Volcanology and Geothermal Research, v. 384, p. 189-205.

Bonali, F. L., Corti, N., Mariotto, F. P., De Beni, E., Bressan, S., Cantarero, M., Russo, E., Neri, M., and Tibaldi, A., 2024, 3D study of dyke-induced asymmetric graben: the 1971 Mt. Etna (Italy) case by structural data and numerical modelling: Journal of Structural Geology, p. 105231.

Byerlee, J., 1978, Friction of Rocks: Pure and Applied Geophysics, v. 116, no. 4-5, p. 615-626.

Calais, E., d'Oreye, N., Albaric, J., Deschamps, A., Delvaux, D., Deverchere, J., Ebinger, C., Ferdinand, R. W., Kervyn, F., Macheyeki, A. S., Oyen, A., Perrot, J., Saria, E., Smets, B., Stamps, D. S., and Wauthier, C., 2008, Strain accommodation by slow slip and dyking in a youthful continental rift, East Africa: Nature, v. 456, no. 7223, p. 783-787.

Casey, M., Ebinger, C., Keir, D., Gloaguen, R., and Mohamed, F., 2006, Strain accommodation in transitional rifts: extension by magma intrusion and faulting in Ethiopian rift magmatic segments: Afar Volcanic Province within the East African Rift System, v. 259, no. 1, p. 143-+.

Chadwick, W. W., and Embley, R. W., 1998, Graben formation associated with recent dike intrusions and volcanic eruptions on the mid-ocean ridge: Journal of Geophysical Research: Solid Earth, v. 103, no. B5, p. 9807-9825.

Drymoni, K., Russo, E., Tibaldi, A., Corti, N., Bonali, F. L., and Mariotto, F. P., 2023, Dyke-induced graben formation in a heterogeneous succession on Mt. Etna: Insights from field observations and FEM numerical models: Journal of Volcanology and Geothermal Research, v. 433, p. 107712.

Dumont, S., Klinger, Y., Socquet, A., Doubre, C., and Jacques, E., 2017, Magma influence on propagation of normal faults: Evidence from cumulative slip profiles along Dabbahu-Manda-Hararo rift segment (Afar, Ethiopia): Journal of Structural Geology, v. 95, p. 48-59.

Dumont, S., Socquet, A., Grandin, R., Doubre, C., and Klinger, Y., 2016, Surface displacements on faults triggered by slow magma transfers between dyke injections in the 2005-2010 rifting episode at Dabbahu-Manda-Hararo rift (Afar, Ethiopia): Geophysical Journal International, v. 204, no. 1, p. 399-417.

Ebinger, C. J., and Casey, M., 2001, Continental breakup in magmatic provinces: An Ethiopian example: Geology, v. 29, no. 6, p. 527-530.

Grandin, R., Socquet, A., Binet, R., Klinger, Y., Jacques, E., de Chabalier, J. B., King, G., Lasserre, C., Tait, S., and Tapponnier, P., 2009, September 2005 Manda Hararo-Dabbahu rifting event, Afar (Ethiopia): Constraints provided by geodetic data: Journal of Geophysical Research: Solid Earth (1978–2012), v. 114, no. B8.

Grandin, R., Socquet, A., Jacques, E., Mazzoni, N., De Chabalier, J. B., and King, G., 2010, Sequence of rifting in Afar, Manda-Hararo rift, Ethiopia, 2005–2009: Time-space evolution and interactions between dikes from interferometric synthetic aperture radar and static stress change modeling: Journal of Geophysical Research: Solid Earth, v. 115, no. B10.

Hamling, I., 2010, Measuring and modelling deformation during the Dabbahu (Afar) rifting episode: University of Leeds.

Hamling, I. J., Ayele, A., Bennati, L., Calais, E., Ebinger, C. J., Keir, D., Lewi, E., Wright, T. J., and Yirgu, G., 2009, Geodetic observations of the ongoing Dabbahu rifting episode: new dyke intrusions in 2006 and 2007: Geophysical Journal International, v. 178, no. 2, p. 989-1003.

Hjartardóttir, Á. R., Einarsson, P., Bramham, E., and Wright, T. J., 2012, The Krafla fissure swarm, Iceland, and its formation by rifting events: Bulletin of Volcanology, v. 74, no. 9, p. 2139-2153.

Hofmann, B., 2013, How do faults grow in magmatic rifts? LiDAR and InSAR observations of the Dabbahu rift segment, Afar, Ethiopia, University of Leeds.

Li, Y., Pusok, A. E., Davis, T., May, D. A., and Katz, R. F., 2023, Continuum approximation of dyking with a theory for poro-viscoelastic–viscoplastic deformation: Geophysical Journal International, v. 234, no. 3, p. 2007-2031.

Magee, C., and Jackson, C. A.-L., 2021, Can we relate the surface expression of dike-induced normal faults to subsurface dike geometry?: Geology, v. 49, no. 4, p. 366-371.

Magee, C., and Jackson, C. A. L., 2020, Seismic reflection data reveal the 3D structure of the newly discovered Exmouth Dyke Swarm, offshore NW Australia: Solid Earth, v. 11, no. 2, p. 579-606.

Mastin, L. G., and Pollard, D. D., 1988, Surface Deformation and Shallow Dike Intrusion Processes at Inyo Craters, Long Valley, California: Journal of Geophysical Research-Solid Earth and Planets, v. 93, no. B11, p. 13221-13235.

Nissen, E., Krishnan, A. K., Arrowsmith, J. R., and Saripalli, S., 2012, Three-dimensional surface displacements and rotations from differencing pre-and post-earthquake LiDAR point clouds: Geophysical Research Letters, v. 39, no. 16.

Pallister, J. S., McCausland, W. A., Jonsson, S., Lu, Z., Zahran, H. M., El Hadidy, S., Aburukbah, A., Stewart, I. C. F., Lundgren, P. R., White, R. A., and Moufti, M. R. H., 2010, Broad accommodation of rift-related extension recorded by dyke intrusion in Saudi Arabia: Nature Geoscience, v. 3, no. 10, p. 705-712.

Pollard, D. D., Delaney, P. T., Duffield, W. A., Endo, E. T., and Okamura, A. T., 1983, Surface Deformation in Volcanic Rift Zones: Tectonophysics, v. 94, no. 1-4, p. 541-584.

Rotevatn, A., Jackson, C. A.-L., Tvedt, A. B., Bell, R. E., and Blækkan, I., 2019, How do normal faults grow?: Journal of Structural Geology, v. 125, p. 174-184.

Rowland, J., Baker, E., Ebinger, C., Keir, D., Kidane, T., Biggs, J., Hayward, N., and Wright, T., 2007, Fault growth at a nascent slow-spreading ridge: 2005 Dabbahu rifting episode, Afar: Geophysical Journal International, v. 171, no. 3, p. 1226-1246.

Rubin, A. M., 1992, Dike-induced faulting and graben subsidence in volcanic rift zones: Journal of Geophysical Research: Solid Earth, v. 97, no. B2, p. 1839-1858.

Rubin, A. M., and Pollard, D. D., 1988, Dike-Induced Faulting in Rift Zones of Iceland and Afar: Geology, v. 16, no. 5, p. 413-417.

Ruch, J., Wang, T., Xu, W., Hensch, M., and Jonsson, S., 2016, Oblique rift opening revealed by reoccurring magma injection in central Iceland: Nat Commun, v. 7, p. 12352.

Trippanera, D., Acocella, V., Ruch, J., and Abebe, B., 2015a, Fault and graben growth along active magmatic divergent plate boundaries in Iceland and Ethiopia: Tectonics, v. 34, no. 11, p. 2318-2348.

Trippanera, D., Ruch, J., Acocella, V., and Rivalta, E., 2015b, Experiments of dike-induced deformation: Insights on the long-term evolution of divergent plate boundaries: Journal of Geophysical Research: Solid Earth, v. 120, no. 10, p. 6913-6942.

Vye-Brown, C., Medynski, S., Smith, K., Field, L., and Wright, T., 2012, Geological map of the Dabbahu (Manda-Hararo) Rift, North, 1:100,000 scale: British Geological Survey.

Walker, J. F., Roberts, G. P., Cowie, P., Papanikolaou, I. D., Sammonds, P., Michetti, A., and Phillips, R., 2009, Horizontal strain-rates and throw-rates across breached relay zones, central Italy: Implications for the preservation of throw deficits at points of normal fault linkage: Journal of Structural Geology, v. 31, no. 10, p. 1145-1160.

Walsh, J. J., Bailey, W. R., Childs, C., Nicol, A., and Bonson, C. G., 2003, Formation of segmented normal faults: a 3-D perspective: Journal of Structural Geology, v. 25, no. 8, p. 1251-1262.

Wright, T. J., Ebinger, C., Biggs, J., Ayele, A., Yirgu, G., Keir, D., and Stork, A., 2006, Magma-maintained rift segmentation at continental rupture in the 2005 Afar dyking episode: Nature, v. 442, no. 7100, p. 291-294.

Wright, T. J., Sigmundsson, F., Pagli, C., Belachew, M., Hamling, I. J., Brandsdottir, B., Keir, D., Pedersen, R., Ayele, A., Ebinger, C., Einarsson, P., Lewi, E., and Calais, E., 2012, Geophysical constraints on the dynamics of spreading centres from rifting episodes on land: Nature Geoscience, v. 5, no. 4, p. 242-250.

Hofmann et al.
Figure 1

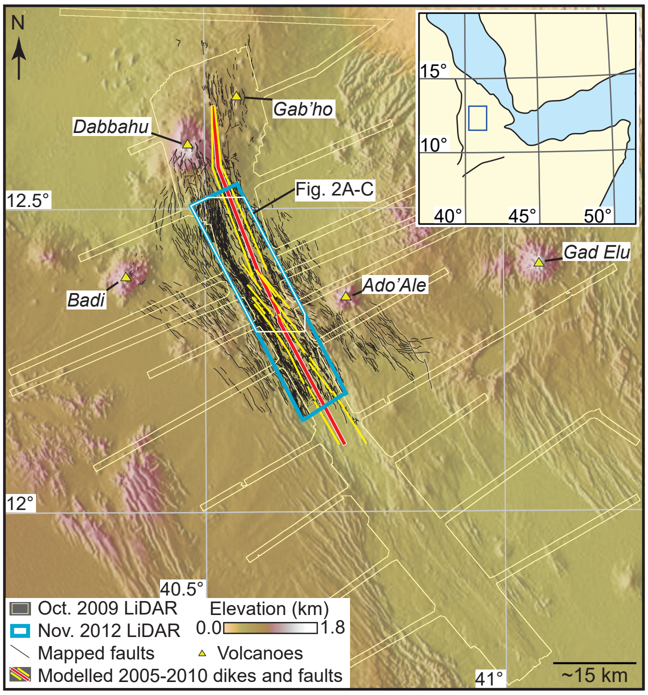

Hofmann et al.
Figure 2

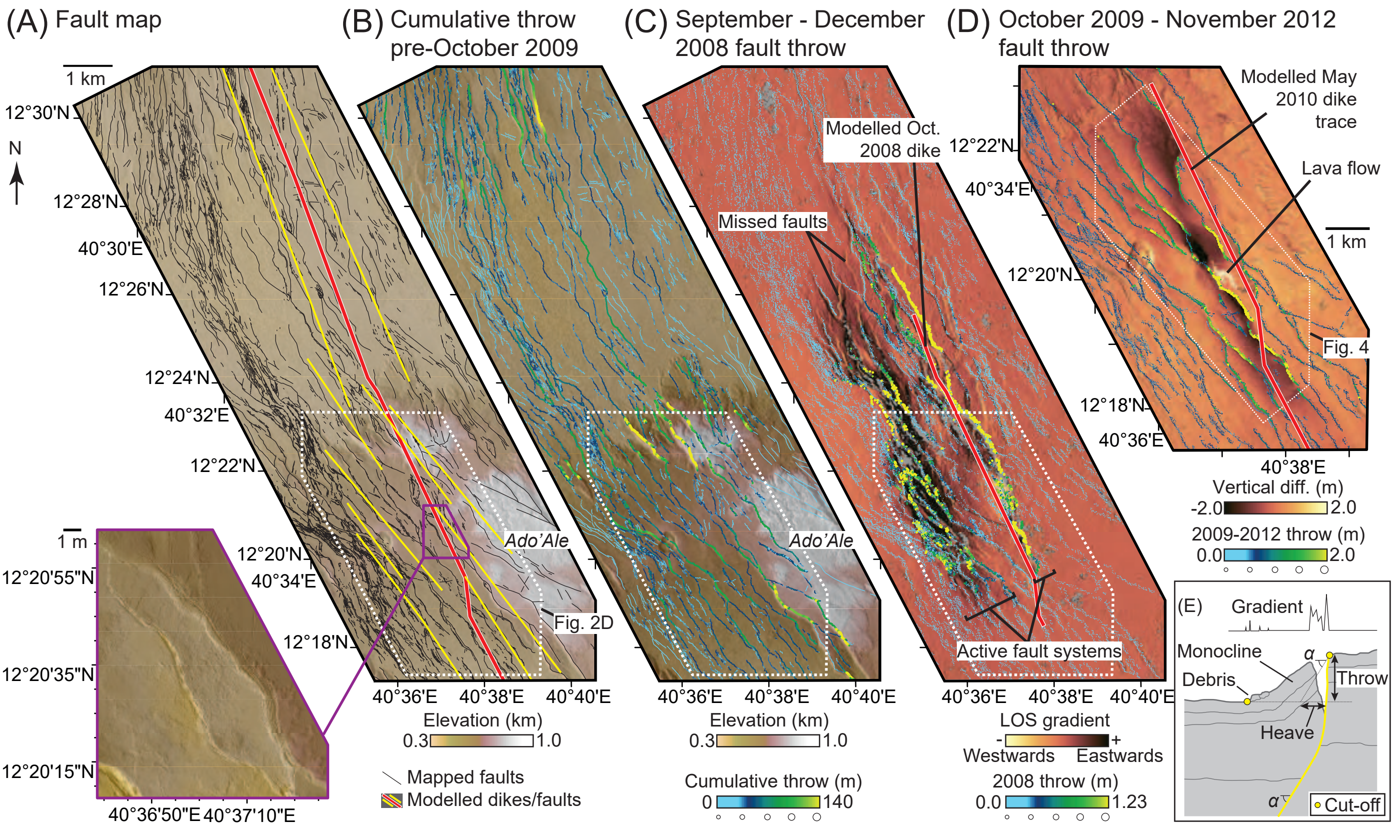

Figure 3

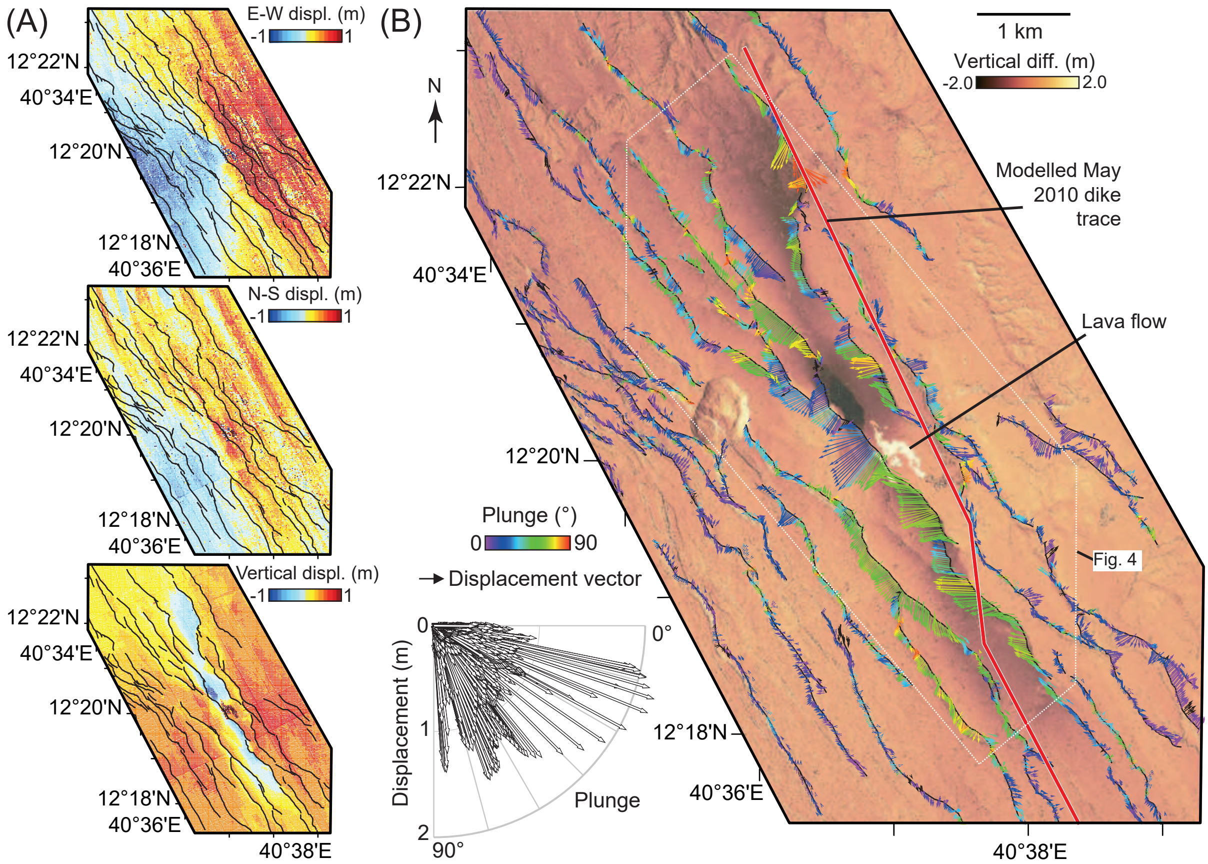

(A)
E-W displ. (m)
-1
1
12°22'N
40°34'E
12°20'N
12°18'N
40°36'E
N-S displ. (m)
-1
1
12°22'N
40°34'E
12°20'N
12°18'N
40°36'E
Vertical displ. (m)
-1
1
12°22'N
40°34'E
12°20'N
12°18'N
40°36'E
40°38'E
(B)
1 km
Vertical diff. (m)
-2.0
2.0
N
12°22'N
40°34'E
Modelled May 2010 dike trace
Lava flow
12°20'N
Plunge (°)
0
90
Displacement vector
Fig. 4
0
1
2
Displacement (m)
0°
90°
Plunge
12°18'N
40°36'E
40°38'E

Hofmann et al.
Figure 4

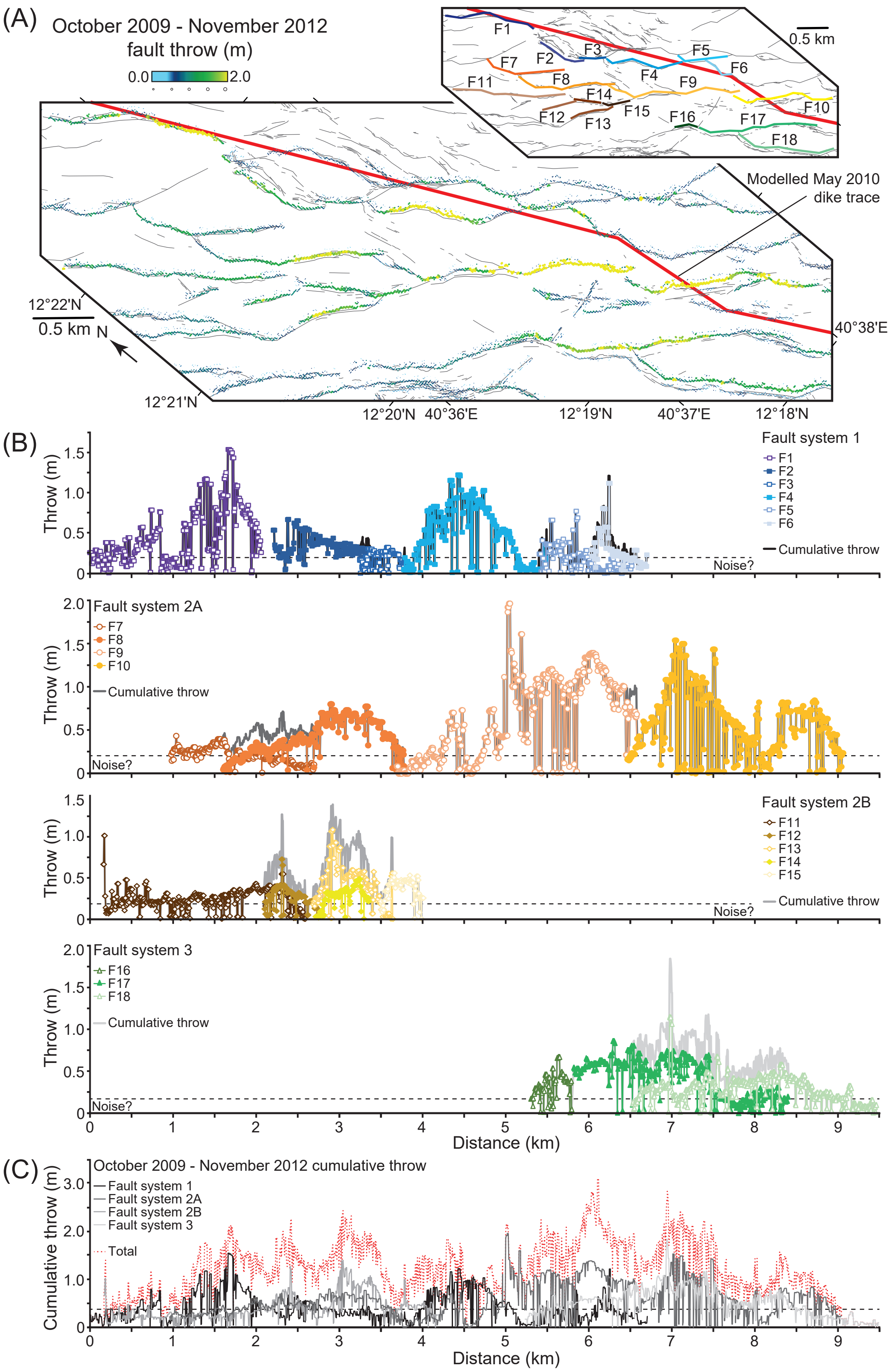

Supplementary Text

Throw distribution across the Dabbahu-Manda Hararo dike-induced fault array: implications for rifting and faulting

Barbara Hofmann[1], Craig Magee[2], Tim J Wright[2]

[1]HR Wallingford, Howbery Park, Wallingford, UK

[2]COMET, School of Earth and Environment, University of Leeds, UK

Data and Methods

We use InSAR and LiDAR data that image the Dabbahu-Manda Hararo magmatic segment. With the InSAR data, we focus on the October 2008 dike event and use track 499 Advanced Land Observing Satellite (ALOS) acquisitions, obtained on 14 September and 15 December 2008, to extract line of site (LOS) displacement trends of the surface at 20 m resolution (Fig. 2C) (Hofmann, 2013). From an unwrapped interferogram comparing these acquisitions (Supplementary Fig. S2), we calculate the LOS displacement gradient for the E-W direction in which linear zones of high gradient represent faults. The two LiDAR surveys we use were acquired in October 2009 and November 2012 by the UK Natural Environment Research Council's Airborne Research and Survey Facility (Hofmann, 2013). We converted each LiDAR survey into digital elevation models (DEM), which have 0.5 m pixel resolutions and vertical accuracies of 0.2 m (Barnie et al., 2016; Hofmann, 2013). Using the original LiDAR point cloud data, we applied an Iterative Closest Point (ICP) algorithm to isolate the vertical and horizontal (in E-W and N-S directions) differences between the 2009 and 2012 surveys;

combining these allow us to calculate the 3D displacement field related to the May 2010 dike event (e.g. Nissen et al., 2012).

We develop an algorithm that identifies fault hanging wall and footwall cut-offs from changes in LOS displacement or elevation gradients on across-fault profiles. These profiles are 600 m long across and oriented orthogonal to the average strike of each fault at 20 m intervals (Hofmann, 2013). Footwall cut-offs are well defined but true hanging wall cut-offs are often obscured by monoclines or debris. Our algorithm considers all gradient changes along the hanging wall and assesses differences between their LOS displacements or elevations, as well as those of the footwall cut-off. We assume hanging wall cut-offs should have gradients >0.5 and show reasonable displacement or elevation changes relative to the footwall cut-off or those within monoclines or debris, but not compared to any along the graben floor (Hofmann, 2013). Throw is calculated from the identified faults cut-offs but heave, and thus displacement, cannot always be accurately defined where monoclines and debris are present. For the InSAR data, our throw calculation assumes faults are pure dip-slip, dip at 65°, and strike at either 150° if they are west-dipping or -30° if east-dipping (Hofmann, 2013). To account for various sources of noise in our datasets, we conservatively consider throw values <20 cm may be erroneous.

References

Barnie, T., Keir, D., Hamling, I., Hofmann, B., Belachew, M., Carn, S., Eastwell, D., Hammond, J. O., Ayele, A., and Oppenheimer, C., 2016, A multidisciplinary study of the final episode of the Manda Hararo dyke sequence, Ethiopia, and implications for trends in volcanism during the rifting cycle: Geological Society, London, Special Publications, v. 420, no. 1, p. 149-163.

Hofmann, B., 2013, How do faults grow in magmatic rifts? LiDAR and InSAR observations of the Dabbahu rift segment, Afar, Ethiopia, University of Leeds. https://etheses.whiterose.ac.uk/7546/

Nissen, E., Krishnan, A. K., Arrowsmith, J. R., and Saripalli, S., 2012, Three-dimensional surface displacements and rotations from differencing pre-and post-earthquake LiDAR point clouds: Geophysical Research Letters, v. 39, no. 16.

Supplementary figure 1

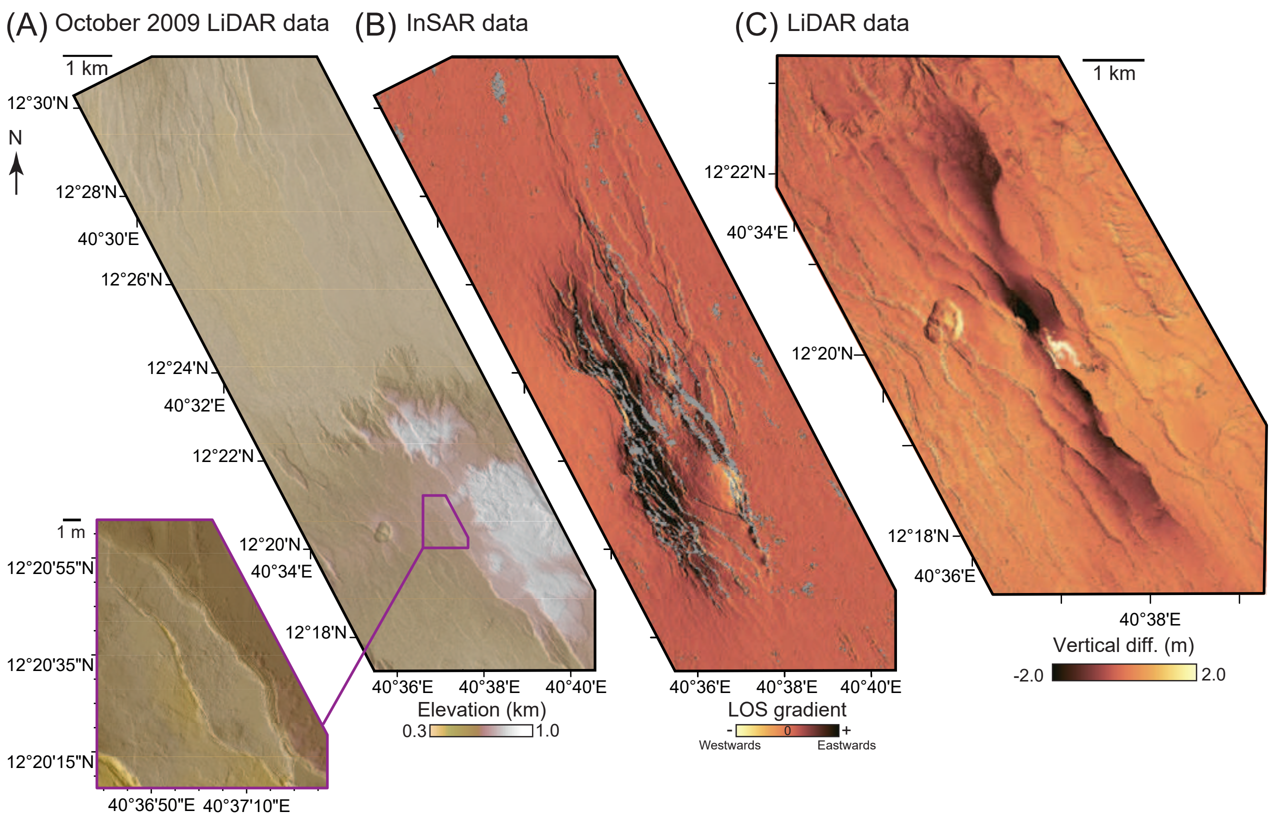

Figure S1: Uninterpreted images of the October 2009 LiDAR survey (A), Advanced Land Observing Satellite (ALOS) interferogram from track 499 (acquired on 14 September and 15 December 2008) estimating the line of site (LOS) displacement trends of the surface during the 2008 diking event (B), and the vertical difference between the 2009 and 2012 LiDAR datasets presented in Figure 2. Grey in B indicates areas of no data.

Supplementary Figure 2

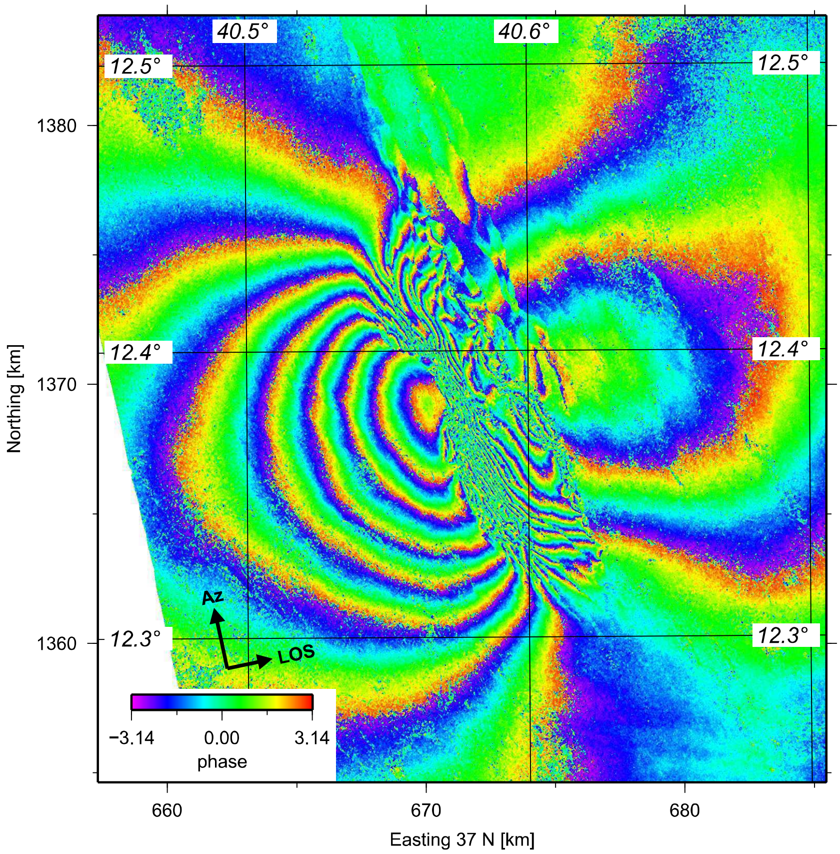

Figure S2: Advanced Land Observing Satellite (ALOS) interferogram from track 499 comparing acquisitions on 14th September and 15th December 2008). Az is the satellite flight direction and LOS the look direction.